Difference in biophysical properties of cancer-initiating cells in melanoma mutated zebrafish

N. Makarova[1#], Vivek Kalaparthi, [1,#,†], Andrew Wang[1, ††], Chris Williams[1, †††], M. E. Dokukin[1,2], Charles Kaufman [3], Leonard Zon [4], I. Sokolov[1,5,6 *]

[1] Department of Mechanical Engineering, Tufts University, Medford, MA, USA

[2] Sarov Physical and Technical Institute, National Research Nuclear University MEPhI, Sarov, Russian Federation

[3] Department of Medicine, Division of Oncology, Washington University, St. Louis, MO, USA

[4] Boston Children's Hospital, Boston, MA, USA

[5] Department of Biomedical Engineering, Tufts University, Medford, MA, USA

[6] Department of Physics, Tufts University, Medford, MA, USA

[†] Present address: Global Foundary, Essex Junction, VT 05452, USA

[††] Present address: Department of Physics, Harvard University, MA USA.

[†††] Present address: Johns Hopkins University, Baltimore, MD, USA

# Equal contribution

* igor.sokolov@tufts.edu

Abstract

Despite sharing oncogenetic mutations, only a small number of cells within a given tissue will undergo malignant transformation. Biochemical and physical factors responsible for this cancer-initiation process are not well understood. Here we study biophysical differences of pre-melanoma and melanoma cells in a $BRAF^{V600E}$ / P53 zebrafish model. The AFM indentation technique was used to study the cancer-initiating cells while the surrounding melanocytes were the control. We observed a statistically significant decrease in the modulus of elasticity (the effective Young's modulus) of cancer-initiating cells compared to the surrounding melanocytes. No significant differences in the pericellular coat surrounding cells were observed. These results contribute to a better understanding of the factors responsible for the initiation of cancer.

Keywords: Cell mechanics; Initiation of cancer; Atomic force microscopy; Pericellular coat; Zebrafish

1. Introduction

The problem of "zero time" of cancer emergence is one of the main challenges in modern cancer study. It is known that there are many cancer-prone cells in an organ, but only a few of them are converted into a malignant state (Almassalha et al., 2016; Slaughter et al., 1953; Sokolov et al., 2018; Tsui et al., 2009). It has been recently shown that a tumor can begin from presumably a single cell within a cluster of precancerous cells that share oncogenetic mutation (Kaufman et al., 2016). To demonstrate this, a zebrafish melanoma model was used, in which the human $BRAF^{V600E}$ oncogene was driven by the melanocyte-specific *p53* mutant loss-of-function background (termed $BRAF^{V600E}$ / P53 zebrafish) (Patton et al., 2005). To visualize a tumor initiation, a fluorescent *crestin:EGFP* reporter was developed (Kaufman et al., 2016). Because the zebrafish crestin gene is specifically expressed only in melanoma tumors of adult zebrafish, it was possible to fluorescently detect the initiation of melanoma tumors directly in zebrafish in vivo by monitoring the expression of GFP under the control of the transcriptional regulatory elements (promoter/enhancer) for crestin. It was observed that tumors were initiated only in a rather small number of cells for the duration of several months despite the presence of thousands of melanocytes sharing the potentially cancer-causing BRAF/p53 mutations. This indicates that other factors that are not well understood are also essential for tumor initiation. The main question is why a particular cell is reprogrammed for malignant behavior, while genetically similar neighbor cells are not. Physical properties of cells might be one of such factors. These properties are studied in the present work.

In the present work, we study the difference in physical properties of cancer-initiating and surrounding melanocytes extracted directly from tumors of $BRAF^{V600E}$ / P53 zebrafish. The study of the physical properties of cells, its mechanics, is an active area of research (Li et al., 2018; Simon et al., 2016; Wu et al., 2018), in particular, in connection with cancer. Mechanical properties of cells are important factors that define cell functionality, motility, tissue formation (Galbraith and Sheetz, 1998; Vogel and Sheetz, 2006), and stem cell differentiation (Chaudhuri and Mooney). Low rigidity of the majority of cancer cells was recently suggested to be used for cancer diagnosis (Cross et al., 2011; Lekka and Laidler, 2009; Paszek et al., 2005). Atomic force microscope (AFM) is one of the popular methods to study cell mechanics (Ani et al., 2019; Dufrene et al., 2013; Haase and Pelling, 2015; Virjula et al., 2017; Wu et al., 2018). It has recently been shown that the AFM indentation allows extracting information not only about cell mechanics but also about the pericellular coat or brush-like layer surrounding eukaryotic and the majority of prokaryotic cells (Boehm et al., 2009; Simon et al., 2016; Sokolov and Dokukin, 2018b;

Targosz-Korecka et al., 2017). Furthermore, as was demonstrated in (Guz et al., 2014), ignoring the mechanical contribution of the pericellular coat leads to incorrect estimation of the elastic modulus of the cell body for many cell phenotypes.

To take into account the presence of the pericellular coat, here we use the AFM method developed in (Sokolov and Dokukin, 2018a; Sokolov et al., 2013), the brush model. This model allows to separate and study the elastic modulus of the cell body and physical properties of the pericellular coat surrounding cells. The model takes into account the non-Hertzian behavior of the pericellular layer. As was demonstrated (Guz et al., 2014), the brush model allowed extraction of the elastic modulus of the cell body in a self-consistent, depth-independent manner. Using the brush model, a statistically significant difference between the elastic modulus of the cell body of cancer-initiating cells and the control is observed for each animal. At the same time, there are no consistent and significant differences in the pericellular coat found. Further, we demonstrate that the use of the particular AFM method is important to observe the reported differences. The use of the standard Hertz model, which is frequently used to analyze the AFM force-indentation curves, fails to confirm the statistically significant difference in the elastic modulus for each fish. Furthermore, we show that the strong linearity principle, independence of the elastic modulus on the indentation depth is valid only for the brush model. The reported results are compared to the previously reported studies of cell mechanics during progression to cancer. The reasons for the observed softness of cancer-initiating cells is briefly discussed.

2. Materials and methods

2.1. Melanoma Tumor Cell Isolation

After humane euthanasia of the zebrafish, a spontaneously arising crestin: GFP + melanoma tumor with some adjacent melanocytes was excised with a scalpel and dissociated mechanically with a razor blade followed by treatment with 50% Ham's F12/50% DMEM, 10× Pen/Strep, 0.075 mg/mL Liberase for 30 minutes. The reaction was stopped with 50% Ham's F12/50% DMEM, 10× Pen/Strep, 15% heat-inactivated fetal calf serum. After filtering through a 40-micron mesh filter, cells were plated on a 60 mm plastic petri dish coated with fibronectin and grown in zebrafish complete medium until imaging (cite Heilman et al, White R, Cancer Research, 2015). Adjacent pigmented melanocytes served as the control. GFP + cells are tumors cells. Pigmented, non-GFP+ cells are normal melanocytes. Non-

pigmented, non-GFP+ cells were a mix of skin cells/endothelial cells/blood that will unavoidably be collected during dissection and were ignored for this analysis.

2.2. Atomic force microscopy

Bioscope Catalyst (Bruker, Inc., CA) AFM placed on Nikon U2000 confocal Eclipse C1 microscope and Dimension 3100 (Bruker Nano/Veeco, Inc.) AFM with Nanoscope V controller and nPoint close-loop scanner (200 μm × 200 μm × 30 μm, XYZ) were used in the present study. It should be noted that a large vertical close-loop Z-range was particularly important because the cell height was ~10 μm. Adding the ramp size needed to collect the force curves, one can easily get a number required for the Z-scan range (ramp size) close to the full extent of the scanner. The close-loop is important for a quantitative description of the force curves with such an extended scan range. A standard cantilever holder for operation in liquids were employed. The raw indentation data were collected with the vertical ramp size of 5-6 μm. To minimize viscoelastic effects, the indentation data were recorded at a frequency of 2Hz. While it is impossible to avoid the viscoelastic effects completely, to be consistent, we performed all measurements with the same oscillation frequency of 2Hz. The AFM software used were versions 5.12, release 4 and 7.12. The data were also pre-processed to align the baseline with SPIP (Image Metrology A/S).

The force-volume images of cells were collected with the resolution of 16x16 pixels (typically within 50 x 50 μm^2 area). Standard V-shaped arrow 200 μm AFM tipless cantilevers (Veeco, Santa Barbara, CA) were used throughout the study. The cantilever spring constant was measured using the thermal tuning method before gluing the spherical probe. A 5 μm diameter silica balls (Bangs Labs, Inc.) were glued to the cantilevers as described in (Berdyyeva et al., 2005). The radius of the probe was measured by imaging the inverse grid (TGT1 by NT-NGT, Russia). The use of a rather AFM dull probe is important to attain self-consistency of the used models. As was shown in (Guz et al., 2014), the use of a sharp commercial AFM probe doesn't allow to satisfy the necessary condition for self-consistency, depth independence of the obtained modulus. It is worth noting that the use of a parabolic probe of ~600nm in radius seems to give the same value of the modulus as the 5 μm silica ball (Wu et al., 2018).

In each experiment, the AFM cantilever sensitivity was calibrated against a rigid substrate, a small piece of a silicon wafer or cover slide immersed in the PBS solution in the Petri dish. Performing the sensitivity calibration tests, we also check if the AFM probe has any possible contamination. For example, if the

silica ball was covered with a noticeable organic contaminant, it would be immediately seen on the calibration force curves. Specifically, the calibration curves (deflection of the cantilever versus vertical displacement of the scanner) would no longer have a sharp well-defined contact, which is seen when using a clean probe. If the contamination was detected, the probe was changed. In some cases, it was possible to clean the probe in acid/base solutions or with water plasma. The radius of the probe and its initial cleanliness were tested by AFM scanning the reversed grid (TGT1, NT-NGT, Russia). The cantilever spring constant was measured using the built-in option of the Nanoscope software (resonance method and thermal tuning) before gluing the probe.

2.3. AFM mode of operation

To use one of the existing mechanical models, the measurements have to be done right above a spherical-like part of the cell, which typically coincides with the top part of the cell. It is rather hard (if not impossible) to identify such a top part using an optical microscope. Therefore, the force volume mode of AFM operation was used. In this mode, one collects both cell topography and the indentation data (Hassan et al., 1998; Sokolov et al., 2016). Furthermore, the cell topography can be corrected for the inevitable deformation of the cell by the action of the AFM probe (see, ref. (Guz et al., 2014) for detail). We processed the indentation curves collected over the top point of the cell until we reach the inclination angle of 10-15 degree (to collect at least four curves per cell). A few curves were discarded because of their irregular indentation behavior (such curves are always present on cells, which being alive, may probably move during indenting).

3. Theory/calculation

To process the chosen indentation data, we use the brush model (Sokolov and Dokukin, 2018a; Sokolov et al., 2013). This model takes into account the presence of pericellular coat surrounding cells. As was described in the Introduction, the presence and significance of this layer are well-known in biology. The importance of this layer for mechanical characterization of cells has been demonstrated in a series of papers (Guz et al., 2014; Iyer et al., 2009b; Simon et al., 2016). For example, it was shown that the cell body can be approximated as a homogeneous and isotropic material (the elastic modulus of the cell body is weakly dependent on the indentation depth) only when the pericellular brush layer is taken into

account (Guz et al., 2014). Thus, the use of the brush model allows using such mechanical characteristics as the Young's modulus in the instrument independent manner. In addition, the parameter of the pericellular brush layer can also be derived from individual indentation curves. The main idea of the brush model is to take into account the pericellular brush layer, in which mechanical properties are substantially different from the properties of the cell body. Because of that difference, it is possible to separate the elastic contribution of the pericellular layer from the deformation of the cell body itself.

Anatomy of a single indentation curve is shown in Figure 1a. The vertical position of the scanner (Z) is plotted with respect to the reflection of the AFM cantilever (d). Force can be found as the multiplication of the deflection of the cantilever and the cantilever spring constant. In position 1, the AFM probe is far from the cell surface. When the probe starts interacting with the pericellular layer, the AFM cantilever starts deflecting (position 2). Starting from some load force, the pericellular layer is deformed cell much that its stiffness becomes equal to the stiffness of the cell body, and the AFM probe is effectively started deforming the cell body only (position 3). Position 4 shows a high load force in which the cell body is substantially deformed. The brush model uses position 3 on the indentation curve to identify the effective Young's modulus (modulus of elasticity) of the cell body E by processing that part of the indentation curve through the Hertz model. The part of the indentation curve corresponding to position 2 is used to extract the forces due to the pericellular brush, which is characterized using an effective grafting density N and the equilibrium brush length L.

This model is described in detail in (Dokukin et al., 2013; Guz et al., 2014; Sokolov and Dokukin, 2018a; Sokolov et al., 2013). Here we briefly describe its major steps. Figure 1b shows a schematic of the indentation of a cell body covered with a pericellular layer of molecules and membrane protrusions. Geometrical definitions shown in Figure 1b implies the following formula, in which the indentation depth is calculated using the Hertz model:

$$h = Z - Z_0 + \left[\frac{9}{16} \frac{k}{E} \sqrt{\frac{R_{probe} + R_{cell}}{R_{probe} R_{cell}}} \right]^{2/3} d^{2/3} + d \,, \qquad (1)$$

where Z_0 is the position of the undeformed cell body, h is the distance between the AFM probe and the surface of the cell body, E is the elastic (Young's) modulus, k in the spring constant of the AFM cantilever, and R_{probe} (R_{cell}) are the radius of the AFM probe (cell). The Poisson ratio of a cell is chosen to be 0.5 (because of a small range of possible variations of v reported in literature, which is between 0.3

and 0.5, the error in the modulus due to the uncertainty of its definition is small, within 5% (Guz et al., 2014)).

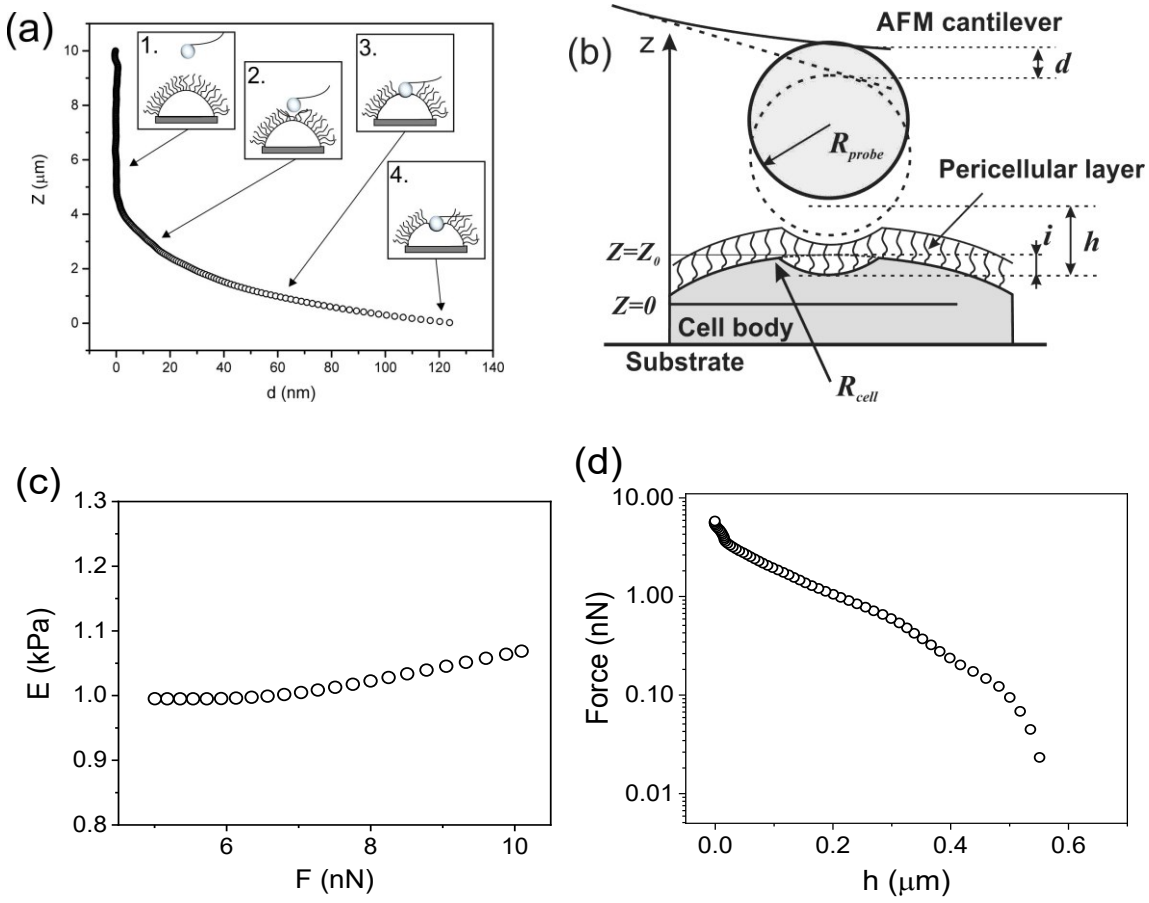

Figure 1. A scheme of the brush model. (a) An example of an indentation curve collected with AFM (the vertical position of the scanner *Z* is plotted with respect to the reflection of the AFM cantilever *d*). Different stages of deformation of a cell by the AFM probe are shown: 1) far away from the surface, 2) touching the pericellular brush layer, 3) deforming mainly the cell body, 4) maximum load force in which the cell body is substantially deformed. (b) A scheme of AFM-cell geometry used in the brush model. R_{probe} (R_{cell}) is the radius of the AFM probe (cell), $\boldsymbol{Z}$ is vertical position of the AFM scanner, $\boldsymbol{d}$ is the cantilever deflection, $\boldsymbol{Z_0}$ is the undeformed position of the cell body, $\boldsymbol{i}$ is deformation of the cell body, $\boldsymbol{Z}$=0 is at the maximum deflection (assigned by the AFM user), and *h* is the separation between the cell body and AFM probe. (c) An example of the dependence of the modules on the load force derived from the indentation curve shown in panel (a). (d) An example of the force due to the brush layer derived from the force curve shown in panel (a).

The indentation curves (*Z* versus *d*) obtained in the AFM indentation experiments are processed in two following steps.

Step 1: Derivation of the elastic (or effective Young's) modulus of the cell body. Assuming the load forces are sufficiently large to almost completely squeeze the brush layer, i.e., h=0, the modulus is calculated from the fit of this part of the indentation curve by using equation (1) in which h=0. Each fitting interval gives the unknown undeformed position of the cell body Z_0 in addition to the modulus of elasticity. In general, one needs to find the region of the indentation curve, in which the indentation force is sufficiently large to substantially squeeze the brush layer and not too large to start detecting heterogeneity of the cell and its substrate. This force region is defined by the presence of a plateau in the modulus dependence on the indentation depth. An example of the modulus plateau is shown in Figure 1c. The size of the plateau depends on the type of cells. Fortunately, the plateau exists for virtually all cells (for least 50% of the indentation curves).

Step 2: Derivation of the force due to the pericellular brush layer. The parameters of this layer, the effective grafting density, and brush length are calculated here. The force due to the presence of the pericellular brush layer can be obtained directly from equation (1) by calculating $h(d)$ and using Hooke's law $F(h) = k \cdot d(h)$. Technically, it is extracted from the experimental data by treating equation (1) as the equation for the inverse function, *h(d)*. Here E and Z_0 are fixed at the plateau values found in Step 1. To find the brush parameters, the effective grafting density and brush length, one needs to characterize the obtained force with equations of Alexander - de Gennes model used for the force of repulsion between a spherical probe of radius R_{probe} and a semi-spherical object of radius R_{cell} and covered with an entropic brush layer (Butt et al., 1999; Iyer et al., 2009a; Sokolov et al., 2007):

$$F(h) \approx 100 k_B T R^* N^{3/2} \exp\left(-2\pi \frac{h}{L}\right) L, \qquad (2)$$

where k_B is the Boltzmann constant, T is the temperature, $R^* = R_{probe} \cdot R_{cell} / (R_{probe} + R_{cell})$, N is the surface density of the brush constituents (grafting density, or effective molecular density), and L is the equilibrium thickness of the brush layer. Note that this formula is valid provided $0.1 < h/L < 0.8$.

Figure 1d shows a representative example of the derived force due to the brush. Note that the force is shown in logarithmic scale. Thus, a straight line in the graph corresponds to the exponential force dependence.

4. Results and Discussion

Since we were working with primary cells derived directly from tumors and surrounding tissue, the cell population may include not only the cells of interest but also other cell types in the skin tissue, for example, keratinocytes and fibroblasts. Because cancer-initiating cells produce green fluorescent protein, such cells were identified using a fluorescent microscope. To identify melanocytes, an optical transmission mode was used because melanocytes contain pigment granules that make them appear darker than other cells. To be able to see both types of cells of interest, the control and cancer-initiating cells were identified using an inverted optical microscope in which fluorescent mode was activated simultaneously with optical transmission mode. A typical optical image is shown in Figure 2. One can see a darker melanocyte and green fluorescent cancer-initiating cells. The optical microscope was combined with a Bruker AFM Bioscope Catalyst. On the top of Fig.2, one can see a dark shadow from the AFM cantilever, which is located above the cells.

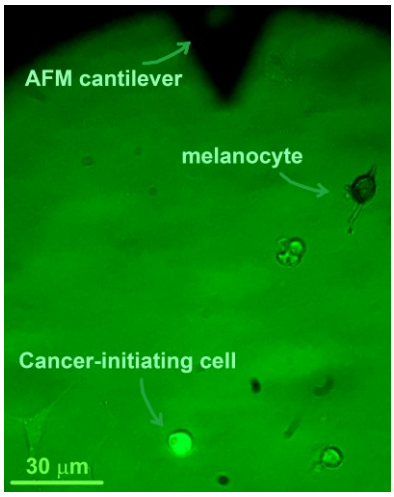

Figure 2. An optical fluorescence/transmission image of cells showing the cancer-initiating cells (green fluorescent) and control melanocytes (dark) cells. An AFM cantilever is also shown.

To study a particular cell, the AFM cantilever is optically positioned above that cell. To obtain the mechanical properties of the cell, the AFM indentation curves were collected over a rectangular area that includes the cell. It is done using the force volume mode, the mode in which AFM collects indentation curves and cell geometry. The latter is important because all existing mechanical models used to extract the elastic parameters of the cell are built on the assumption of known geometry of the cell. Only the

indentation curves close to the cell top were analyzed because we used a mechanical model dealing with a sphere-to-sphere contact (see, the Theory/Calculation section for detail).

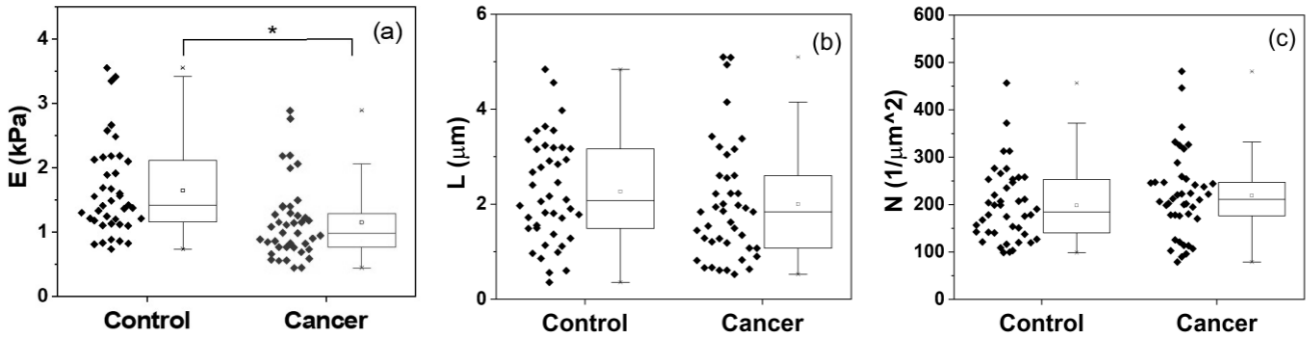

Figure 3. Cell properties obtained from the analysis of individual indentation curves. Each point shows the average value for a single cell. a) The effective Young's modulus (modulus of elasticity), b) the equilibrium length of the pericellular brush layer, c) the accountable grafting density of the pericellular brush layer. The difference in the modulus of elasticity is significant ($p<0.01$).

The cells were collected from 3 different fish. In total, 42 cancer-initiating cells and 40 control cells were studied. Between 4 to 5 indentation curves were analyzed per cell. The results of the data processing are shown in Figure 3. Each point on the graph shows the average value for each cell. This way one avoids uneven contributions from different cells into the total average cell parameters because each cell may have a different number of indentation curves processed. One can see a clear difference in the elastic properties of the cell body (Fig.3a) of the cancer-initiating cells compared to the control. However, there is no no statistically significant difference in either of the brush parameters (Fig.3b,c). One-way ANOVA test confirms that only the modulus of elasticity is significantly different for the cancer-initiating cells compared to control (at $p<0.01$).

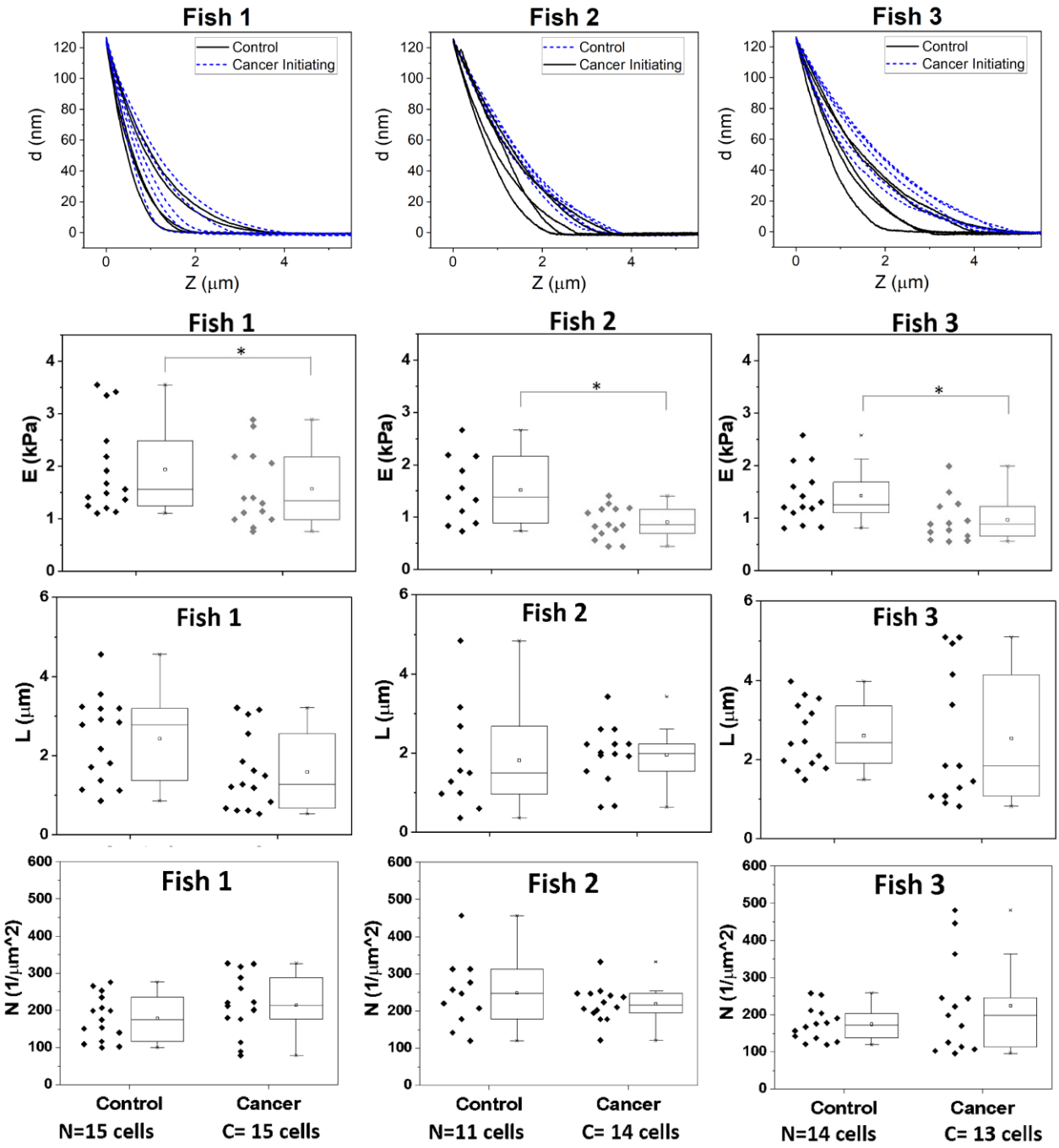

Figure 4. Details of data for individual fish. (Top row): Examples of the indentation curves for each fish. (Bottom rows): The cell parameters calculated for each individual fish. Each point shows the average value for a single cell. The number of cells used in each analysis is shown. The modulus of elasticity (E): The difference in the modulus of elasticity is significant between the control and cancer-initiating cells (at $p<0.01$). The length of the pericellular brush layer (L): The difference in fish 1 is statistically significant at $p<0.05$, whereas fish 2,3 do not :show a

statistically significant difference. The grafting density one of the brush layer (N): No significant difference was observed in either fish.

The observed behavior of the Young's modulus is consistent among all three animals. Figure 4 shows the distributions of the modulus of elasticity for all three animals. One can see that the modulus of elasticity is consistently smaller for the cancer-initiating cells compared to control. The parameters of the brush layer, which are also shown in figure 4, do not show a statistically significant difference (with the exception of the brush length for fish 1; this behavior is not confirmed the other two fish). Figure 4 (top row) shows also representative examples of the indentation curves for each fish for both cancer initiating and control cells.

It is worth noting that the absence of difference in the pericellular brush layer may seem to contradict the previous study of the surface of cancerous cells versus normal cells. For example, a whole series of works on AFM imaging of physical properties of the cell surface showed a substantial change of the cell surface during progression towards cancer (Dokukin et al., 2011; Dokukin et al., 2015b; Guz et al., 2015b; Sokolov, 2015). It was demonstrated on the human cervical cancer model in vitro (Dokukin et al., 2011; Dokukin et al., 2015b; Guz et al., 2015b), and recently, on cells extracted from urine of patients who have active bladder cancer (patients with no bladder cancer were the control group) (Sokolov et al., 2018). The present observations do not indicate the change of the pericellular coat layer on the cells when they become malignant. It should be stressed that our present finding does not contradict the previous results because of two reasons. First, it is a different cell type was considered in the previous studies. Secondly, the results shown in figures 3,4 present different properties of the cell surface. As was demonstrated in (Dokukin et al., 2011; Dokukin et al., 2015b; Guz et al., 2015b; Sokolov, 2015), the observed changes in the surface parameters of malignant cells were at the scale 20-300 nm. At the same time, the physical parameters of the pericellular brush were derived here from the indentation with a 5 μm AFM probe. The present measurements cannot resolve the difference reported in the above references.

There were still similar comparative studies done using an AFM probe of similar size in which the opposite behavior of the effective Young's modulus was observed (Iyer et al., 2009b). There was no statistically significant difference in the mechanical properties of the cell body observed between cancer and normal human cervical epithelial cells. At the same time, a substantial difference in the pericellular brush was found. Nevertheless, we do not consider those results conflicting with the present observations

because of obviously different cell phenotypes. Furthermore, the present control already has oncogenic mutations (BRAFV600E, p53), and therefore, cannot be considered as normal cells. Such a mutation may have a profound effect on the cell surface. A substantial change in physical properties of the surface of human cervical epithelial cells after the oncogenic mutation was demonstrated using nonspecific adhesion of silica particles (Gaikwad et al., 2011; Iyer et al., 2009c) and fractal analysis of the distribution of adhesion or the cell surface (Dokukin et al., 2015a; Guz et al., 2015a).

It may seem that the observed softness of cancer-initiating cells is in agreement with the previously reported softness of cancer cells compared to normal (Cross et al., 2007; Ketene et al., 2012; Lekka et al., 1999; Rebelo et al., 2013). Before answering this question, it should be noted that a different mechanical model was previously used to process data, the Hertz model, which is oversimplified and not self-consistent when applied to cells (Guz et al., 2014). The major problem of using that model is that the obtained Young's modulus depends on the indentation depth (load force). Secondly, most of the previous measurements were done using a sharp AFM probe, which gives the same problem of indentation-dependence even if the brush model is used (Guz et al., 2014; Wu et al., 2018). Moreover, the obtained modulus is substantially higher compared to the one derived when using dull probe indentations (Wu et al., 2018).

To compare our results with the reported previously performed when using the Hertz model, we repeated the previews way of processing the indentation curves, we processed our data with the help of the standard Hertz model while ignoring the presence of the pericellular brush layer. The comparative results are presented in Figures 5 and 6.

Figure 5 shows the average modulus of elasticity and one standard deviation for different load forces (indentation depth). As expected, the brush model shows less depth dependence of the elastic modulus compared to the Hertz model. It is worth noting that the difference between the elastic modulus derived within the Hertz model is not as pronounced as that obtained with the brush model. In particular, the difference in the modulus for fish 1 is not even statistically significant when calculated with the Hertz model. Here we compared the values of the modules at all indentation forces shown in the graph, 6-10 nN. (The difference in the modulus between cancer-initiating and control cells is statistically significant for all other cases.)

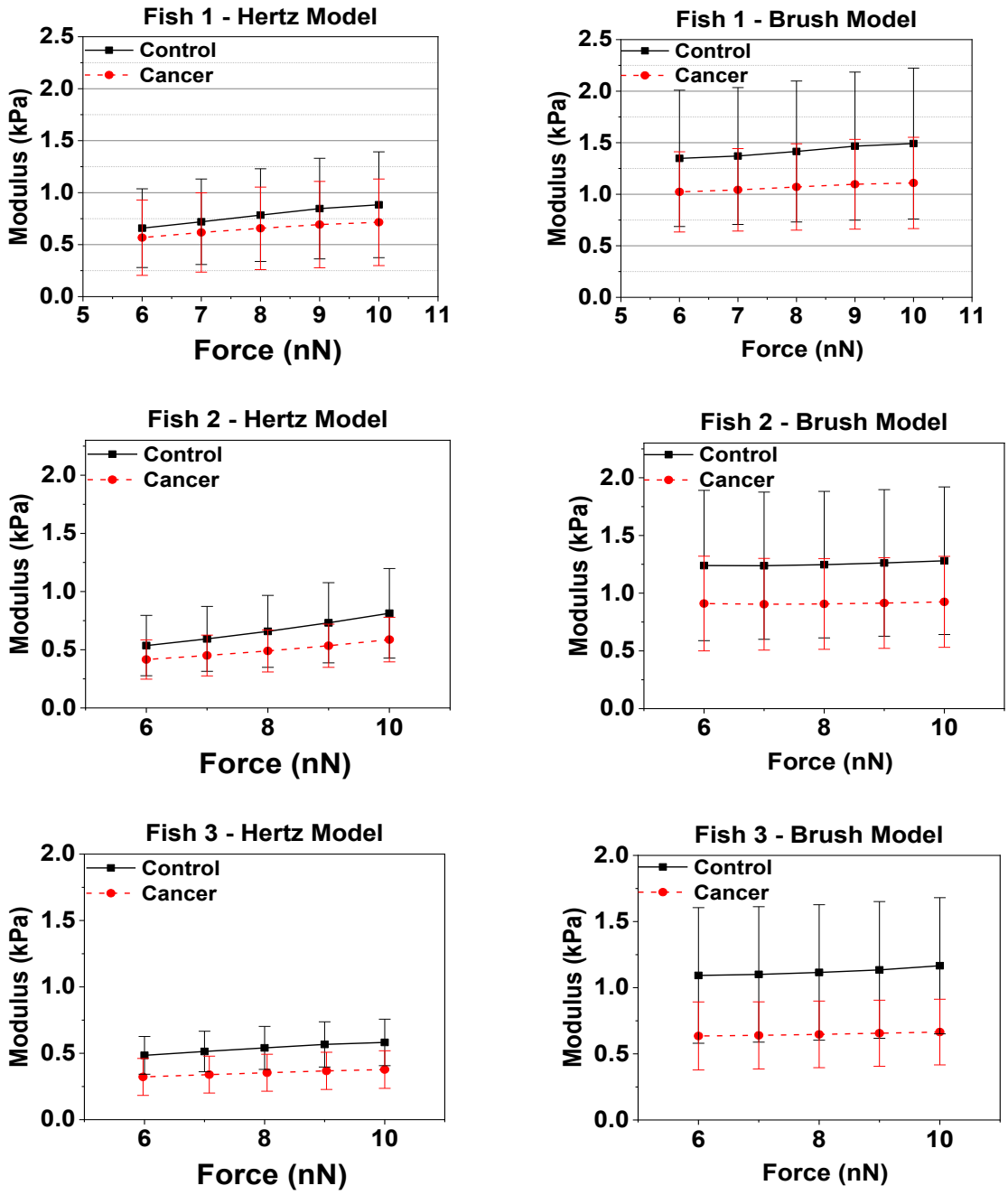

Figure 5. Comparison between the Hertz and brush models used to calculate the modulus of elasticity for cancer-initiating cells and control melanocytes for different load forces. The results for individual fish are shown.

It should be noted that the behavior of the average can be rather misleading because the modulus independence of the indentation depth is needed for each individual indentation, not for the average, see

ref. (Guz et al., 2014) for detail. In brief, the behavior of the average may be substantially different from the behavior of individual indentation curves because we are dealing with a broad distribution of values of the moduli. This also explains a relatively larger standard deviation for modulus derived in the brush model compared to the one derived with the Hertz model (Fig.5). To estimate, we suggest another method. As was shown in (Guz et al., 2014), a better test of the dependence of the modulus on the indentation depth (and consequently, the self-consistency of the used models) is the analysis of the distribution of depth dependency of the modulus calculated for *each* indentation curve. As a measure of depth dependence, it was suggested to calculate the standard deviation of the modulus E from its average for each indentation curve: $St.Dev(E) / Aver(E) \times 100\%$.

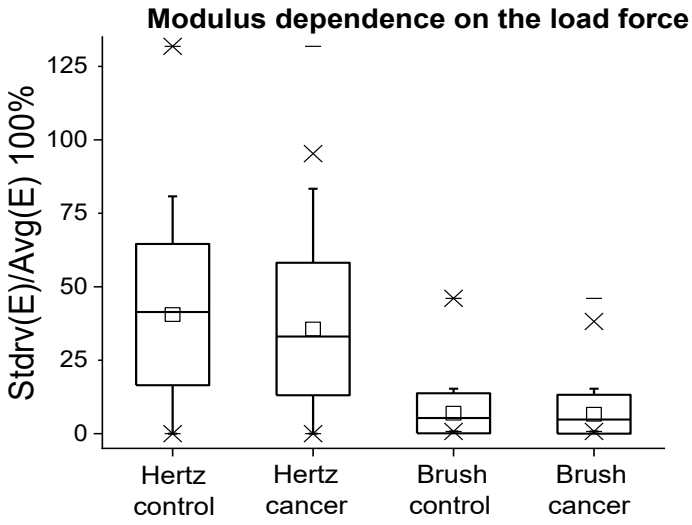

Figure 6. The analysis of depth dependence of the elastic modulus derived within Hertz and brush models. Distributions the measure of depth dependence of the elastic modulus calculated using the brush and Hertz models for both cancer-initiating and control cells. Small values show self-consistency of the brush model.

Zero standard deviation indicates the constancy of the modulus. i.e., its complete depth independence. Figure 6 shows the distributions this measure of depth dependence of the elastic modulus calculated using the brush and Hertz models for both cancer-initiating and control cells. One can see that the brush

model shows much less depth dependence of the modulus, i.e., more self-consistent compared to the Hertz model. It is interesting to note that the percentage of depth dependence is virtually identical to what was calculated in (Guz et al., 2014) for a rather different type of cells.

As one can see from figure 5, the Hertz model qualitatively shows a trend similar to the observed within the brush model, the softening of cancer-initiating cells. Therefore, one can conclude that our observations are, in principle, in agreement with the previously reported softening of malignant cells (Cross et al., 2007; Ketene et al., 2012; Lekka et al., 1999; Rebelo et al., 2013; Sokolov, 2007). Nevertheless, the difference can be not as pronounced as the one derived using the brush model. At the same time, the actual values of the elastic modulus obtained with the Hertz model are noticeably lower, and substantially more depth-dependent. The latter implies, strictly speaking, that the Hertz model cannot be applied to calculate the modules. The fact that the Hertz model gives a noticeably lower value of the modulus comes from the obvious fact that the softer pericellular brush layer is counted in the Hertz model as the cell material. Because the mechanical response of the pericellular brush layer is highly nonlinear (can be approximated as exponential, see the Methods section), it cannot be even considered as a double layer elastic material (Simon et al., 2016).

Finally, it is worthy of discussing the reason for the cells to be softer. As was demonstrated previously (Sokolov et al., 2006; Suresh, 2007; Wu et al., 1998), the elastic properties of cells are defined mainly by the microfilament part of the cytoskeletal, F-actin, in particular, by the level of cross-linking of F-actin (Berdyyeva et al., 2005). One of the simplest explanations of this fact is the fast division of the malignant cells compared to control which may provide insufficient time to develop a higher level of cross-linking (as shown in (Berdyyeva et al., 2005) that the level of cross-linking is increasing with the cell age). However, it is not entirely clear what exactly the role the softening of malignant cells plays in cancer development. At the level of metastasis, softer cells could more easily exit the bloodstream or lymphatic to invade the surrounding tissue, thereby presumably expending less energy in this process. Yet, it is not clear how much the softness of malignant cells is essential in the initial stage of tumor growth. More research is needed to answer this interesting question.

5. Conclusions

Here we reported on the study of biophysical properties of cells that are undergoing the malignant melanoma transformation from nonmalignant cells sharing similar oncogenetic mutations. Cells were directly extracted from tumors and surrounding tissue from three animals. The cells were studied by means of the AFM indentation technique, in which the collected indentation curves were analyzed using the brush model. Our brush model allows to extract the modulus of elasticity of the cell body (the effective Young's modulus) as well as the property of the pericellular coat layer surrounding cells. A statistically significant decrease in the modulus of elasticity of cancer-initiating melanoma cells compared to the surrounding control melanocytes was observed in all three animals. The self-consistency of the brush model was verified through the analysis of the dependence of the derived modulus of elasticity on the indentation depth. A comparison with the classical Hertz model, in which the cell is treated as a homogeneous isotropic linear material, demonstrated that the use of the Hertz model could not be treated as self-consistent. The statistically significant difference in the modulus of elasticity of the cancer-initiating and control cells, which was observed when using the brush model, disappears for one of the animals when the Hertz model was used. These results demonstrate the importance of the use of the brush model which takes into account the mechanical contribution of the pericellular coat layer. The observed physical differences in the mechanics of cancer-initiating cells provide the ground for further study of the role of epigenetic factors responsible for initiating cancer.

Acknowledgments

Support of this work from the National Science Foundation is acknowledged by I.S. (CMMI 1435655, CMMI 1937373) and from the National Institute of Health by L.Z. (R01 CA103846, P01 CA163222).

References

Almassalha, L.M., Bauer, G.M., Chandler, J.E., Gladstein, S., Cherkezyan, L., Stypula-Cyrus, Y., Weinberg, S., Zhang, D., Thusgaard Ruhoff, P., Roy, H.K., Subramanian, H., Chandel, N.S., Szleifer, I., Backman, V., 2016. Label-free imaging of the native, living cellular nanoarchitecture using partial-wave spectroscopic microscopy. Proc Natl Acad Sci U S A 113, E6372-E6381.

Ani, C.J., Obayemi, J.D., Uzonwanne, V.O., Danyuo, Y., Odusanya, O.S., Hu, J., Malatesta, K., Soboyejo, W.O., 2019. A shear assay study of single normal/breast cancer cell deformation and detachment from poly-di-methyl-siloxane (PDMS) surfaces. J Mech Behav Biomed 91, 76-90.

Berdyyeva, T.K., Woodworth, C.D., Sokolov, I., 2005. Human epithelial cells increase their rigidity with ageing in vitro: direct measurements. Physics in Medicine and Biology 50, 81-92.

Boehm, H., Mundinger, T.A., Boehm, C.H.J., Hagel, V., Rauch, U., Spatz, J.P., Curtis, J.E., 2009. Mapping the mechanics and macromolecular organization of hyaluronan-rich cell coats. Soft Matter 5, 4331-4337.

Butt, H.J., Kappl, M., Mueller, H., Raiteri, R., Meyer, W., Ruhe, J., 1999. Steric forces measured with the atomic force microscope at various temperatures. Langmuir 15, 2559-2565.

Chaudhuri, O., Mooney, D.J., STEM-CELL DIFFERENTIATION Anchoring cell-fate cues. Nature Materials 11, 568-569.

Cross, S.E., Jin, Y.S., Lu, Q.Y., Rao, J.Y., Gimzewski, J.K., 2011. Green tea extract selectively targets nanomechanics of live metastatic cancer cells. Nanotechnology 22.

Cross, S.E., Jin, Y.S., Rao, J., Gimzewski, J.K., 2007. Nanomechanical analysis of cells from cancer patients. Nat Nanotechnol 2, 780-783.

Dokukin, M.E., Guz, N.V., Gaikwad, R.M., Woodworth, C.D., Sokolov, I., 2011. Cell surface as a fractal: normal and cancerous cervical cells demonstrate different fractal behavior of surface adhesion maps at the nanoscale. Physical Review Letters 107, 028101.

Dokukin, M.E., Guz, N.V., Sokolov, I., 2013. Quantitative Study of the Elastic Modulus of Loosely Attached Cells in AFM Indentation Experiments. Biophys J 104, 2123-2131.

Dokukin, M.E., Guz, N.V., Woodworth, C.D., Sokolov, I., 2015a. Emergence of fractal geometry on the surface of human cervical epithelial cells during progression towards cancer. New J Phys 17.

Dokukin, M.E., Guz, N.V., Woodworth, C.D., Sokolov, I., 2015b. Emerging of fractal geometry on surface of human cervical epithelial cells during progression towards cancer. New J Phys 17, 033019

Dufrene, Y.F., Martinez-Martin, D., Medalsy, I., Alsteens, D., Muller, D.J., 2013. Multiparametric imaging of biological systems by force-distance curve-based AFM. Nature Methods 10, 847-854.

Gaikwad, R.M., Dokukin, M.E., Iyer, K.S., Woodworth, C.D., Volkov, D.O., Sokolov, I., 2011. Detection of cancerous cervical cells using physical adhesion of fluorescent silica particles and centripetal force. Analyst 136, 1502-1506.

Galbraith, C.G., Sheetz, M.P., 1998. Forces on adhesive contacts affect cell function. Current Opinion in Cell Biology 10, 566-571.

Guz, N., Dokukin, M., Kalaparthi, V., Sokolov, I., 2014. If Cell Mechanics Can Be Described by Elastic Modulus: Study of Different Models and Probes Used in Indentation Experiments. Biophysical Journal 107, 564-575.

Guz, N.V., Dokukin, M.E., Woodworth, C.D., Cardin, A., Sokolov, I., 2015a. Towards early detection of cervical cancer: Fractal dimension of AFM images of human cervical epithelial cells at different stages of progression to cancer. Nanomed-Nanotechnol 11, 1667-1675.

Guz, N.V., Dokukin, M.E., Woodworth, C.D., Cardin, A., Sokolov, I., 2015b. Towards early detection of cervical cancer: Fractal dimension of AFM images of human cervical epithelial cells at different stages of progression to cancer. Nanomedicine 11, 1667-1675.

Haase, K., Pelling, A.E., 2015. Investigating cell mechanics with atomic force microscopy. Journal of the Royal Society Interface 12.

Hassan, A.E., Heinz, W.F., Antonik, M.D., D'Costa, N.P., Nageswaran, S., Schoenenberger, C.A., Hoh, J.H., 1998. Relative microelastic mapping of living cells by atomic force microscopy. Biophys J 74, 1564-1578.

Iyer, S., Gaikwad, R.M., Subba-Rao, V., Woodworth, C.D., Sokolov, I., 2009a. AFM Detects Differences in the Surface Brush on Normal and Cancerous Cervical Cells. Nature Nanotechnology 4, 389-393.

Iyer, S., Gaikwad, R.M., Subba-Rao, V., Woodworth, C.D., Sokolov, I., 2009b. Atomic force microscopy detects differences in the surface brush of normal and cancerous cells. Nature Nanotechnology 4, 389-393.

Iyer, S., Woodworth, C.D., Gaikwad, R.M., Kievsky, Y.Y., Sokolov, I., 2009c. Towards Nonspecific Detection of Malignant Cervical Cells with Fluorescent Silica Beads. Small 5, 2277-2284.

Kaufman, C.K., Mosimann, C., Fan, Z.P., Yang, S., Thomas, A.J., Ablain, J., Tan, J.L., Fogley, R.D., van Rooijen, E., Hagedorn, E.J., Ciarlo, C., White, R.M., Matos, D.A., Puller, A.C., Santoriello, C., Liao, E.C., Young, R.A., Zon, L.I., 2016. A zebrafish melanoma model reveals emergence of neural crest identity during melanoma initiation. Science 351, aad2197.

Ketene, A.N., Schmelz, E.M., Roberts, P.C., Agah, M., 2012. The effects of cancer progression on the viscoelasticity of ovarian cell cytoskeleton structures. Nanomedicine 8, 93-102.

Lekka, M., Laidler, P., 2009. Applicability of AFM in cancer detection. Nat Nanotechnol 4, 72; author reply 72-73.

Lekka, M., Laidler, P., Gil, D., Lekki, J., Stachura, Z., Hrynkiewicz, A.Z., 1999. Elasticity of normal and cancerous human bladder cells studied by scanning force microscopy. Eur Biophys J 28, 312-316.

Li, M., Liu, L.Q., Xu, X.N., Xing, X.J., Dang, D., Xi, N., Wang, Y.C., 2018. Nanoscale characterization of dynamic cellular viscoelasticity by atomic force microscopy with varying measurement parameters. J Mech Behav Biomed 82, 193-201.

Paszek, M.J., Zahir, N., Johnson, K.R., Lakins, J.N., Rozenberg, G.I., Gefen, A., Reinhart-King, C.A., Margulies, S.S., Dembo, M., Boettiger, D., Hammer, D.A., Weaver, V.M., 2005. Tensional homeostasis and the malignant phenotype. Cancer Cell 8, 241-254.

Patton, E.E., Widlund, H.R., Kutok, J.L., Kopani, K.R., Amatruda, J.F., Murphey, R.D., Berghmans, S., Mayhall, E.A., Traver, D., Fletcher, C.D., Aster, J.C., Granter, S.R., Look, A.T., Lee, C., Fisher, D.E., Zon, L.I., 2005. BRAF mutations are sufficient to promote nevi formation and cooperate with p53 in the genesis of melanoma. Curr Biol 15, 249-254.

Rebelo, L.M., de Sousa, J.S., Mendes Filho, J., Radmacher, M., 2013. Comparison of the viscoelastic properties of cells from different kidney cancer phenotypes measured with atomic force microscopy. Nanotechnology 24, 055102.

Simon, M., Dokukin, M., Kalaparthi, V., Spedden, E., Sokolov, I., Staii, C., 2016. Load Rate and Temperature Dependent Mechanical Properties of the Cortical Neuron and Its Pericellular Layer Measured by Atomic Force Microscopy. Langmuir 32, 1111-1119.

Slaughter, D.P., Southwick, H.W., Smejkal, W., 1953. Field cancerization in oral stratified squamous epithelium; clinical implications of multicentric origin. Cancer 6, 963-968.

Sokolov, I., 2007. Atomic force microscopy in cancer cell research. American Scientific Publishers' Inc.

Sokolov, I., 2015. Fractals: a possible new path to diagnose and cure cancer? Future Oncology 11, 3049-3051.

Sokolov, I., Dokukin, M.E., 2018a. AFM Indentation Analysis of Cells to Study Cell Mechanics and Pericellular Coat. Nanoscale Imaging: Methods and Protocols 1814, 449-468.

Sokolov, I., Dokukin, M.E., 2018b. AFM Indentation Analysis of Cells to Study Cell Mechanics and Pericellular Coat. Methods Mol Biol 1814, 449-468.

Sokolov, I., Dokukin, M.E., Guz, N.V., 2013. Method for quantitative measurements of the elastic modulus of biological cells in AFM indentation experiments. Methods 60, 202-213.

Sokolov, I., Dokukin, M.E., Kalaparthi, V., Miljkovic, M., Wang, A., Seigne, J.D., Grivas, P., Demidenko, E., 2018. Noninvasive diagnostic imaging using machine-learning analysis of nanoresolution images of cell surfaces: Detection of bladder cancer. Proceedings of the National Academy of Sciences of the United States of America 115, 12920-12925.

Sokolov, I., Iyer, S., Subba-Rao, V., Gaikwad, R.M., Woodworth, C.D., 2007. Detection of surface brush on biological cells in vitro with atomic force microscopy. Applied Physics Letters 91, 023902-023901-023903.

Sokolov, I., Iyer, S., Woodworth, C.D., 2006. Recovery of elasticity of aged human epithelial cells in vitro. Nanomed-Nanotechnol 2, 31-36.

Sokolov, I., Zorn, G., Nichols, J.M., 2016. A study of molecular adsorption of a cationic surfactant on complex surfaces with atomic force microscopy. Analyst 141, 1017-1026.

Suresh, S., 2007. Biomechanics and biophysics of cancer cells. Acta Biomater 3, 413-438.

Targosz-Korecka, M., Jaglarz, M., Malek-Zietek, K.E., Gregorius, A., Zakrzewska, A., Sitek, B., Rajfur, Z., Chlopicki, S., Szymonski, M., 2017. AFM-based detection of glycocalyx degradation and endothelial stiffening in the db/db mouse model of diabetes. Scientific reports 7, 15951.

Tsui, I.F., Garnis, C., Poh, C.F., 2009. A dynamic oral cancer field: unraveling the underlying biology and its clinical implication. Am J Surg Pathol 33, 1732-1738.

Virjula, S., Zhao, F.H., Leivo, J., Vanhatupa, S., Kreutzer, J., Vaughan, T.J., Honkala, A.M., Viehrig, M., Mullen, C.A., Kallio, P., McNamara, L.M., Miettinen, S., 2017. The effect of equiaxial stretching on the osteogenic differentiation and mechanical properties of human adipose stem cells. J Mech Behav Biomed 72, 38-48.

Vogel, V., Sheetz, M., 2006. Local force and geometry sensing regulate cell functions. Nature Reviews Molecular Cell Biology 7, 265-275.

Wu, H.W., Kuhn, T., Moy, V.T., 1998. Mechanical properties of L929 cells measured by atomic force microscopy: effects of anticytoskeletal drugs and membrane crosslinking. Scanning 20, 389-397.

Wu, P.H., Aroush, D.R.B., Asnacios, A., Chen, W.C., Dokukin, M.E., Doss, B.L., Durand-Smet, P., Ekpenyong, A., Guck, J., Guz, N.V., Janmey, P.A., Lee, J.S.H., Moore, N.M., Ott, A., Poh, Y.C., Ros, R., Sander, M., Sokolov, I., Staunton, J.R., Wang, N., Whyte, G., Wirtz, D., 2018. A comparison of methods to assess cell mechanical properties. Nature Methods 15, 491-498.